

Characterising the atmospheric conditions leading to large error growth in volcanic ash cloud forecasts

Article

Accepted Version

Dacre, H. F. and Harvey, N. J. (2018) Characterising the atmospheric conditions leading to large error growth in volcanic ash cloud forecasts. *Journal of Applied Meteorology and Climatology*. ISSN 1558-8432 doi: <https://doi.org/10.1175/jamc-d-17-0298.1> Available at <http://centaur.reading.ac.uk/75613/>

It is advisable to refer to the publisher's version if you intend to cite from the work.

To link to this article DOI: <http://dx.doi.org/10.1175/jamc-d-17-0298.1>

Publisher: American Meteorological Society

All outputs in CentAUR are protected by Intellectual Property Rights law, including copyright law. Copyright and IPR is retained by the creators or other copyright holders. Terms and conditions for use of this material are defined in the [End User Agreement](#).

www.reading.ac.uk/centaur

CentAUR

Central Archive at the University of Reading

Reading's research outputs online



AMERICAN METEOROLOGICAL SOCIETY

Journal of Applied Meteorology and Climatology

EARLY ONLINE RELEASE

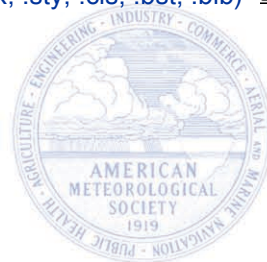
This is a preliminary PDF of the author-produced manuscript that has been peer-reviewed and accepted for publication. Since it is being posted so soon after acceptance, it has not yet been copyedited, formatted, or processed by AMS Publications. This preliminary version of the manuscript may be downloaded, distributed, and cited, but please be aware that there will be visual differences and possibly some content differences between this version and the final published version.

The DOI for this manuscript is doi: [10.1175/JAMC-D-17-0298.1](https://doi.org/10.1175/JAMC-D-17-0298.1)

The final published version of this manuscript will replace the preliminary version at the above DOI once it is available.

If you would like to cite this EOR in a separate work, please use the following full citation:

Dacre, H., and N. Harvey, 2018: Characterising the atmospheric conditions leading to large error growth in volcanic ash cloud forecasts. *J. Appl. Meteor. Climatol.* doi:[10.1175/JAMC-D-17-0298.1](https://doi.org/10.1175/JAMC-D-17-0298.1), in press.



1 **Characterising the atmospheric conditions leading to large error growth in**
2 **volcanic ash cloud forecasts**

3 H.F.Dacre* and N.J.Harvey†

4 *Department of Meteorology, University of Reading, Earley Gate, PO Box 243, Reading, RG6*
5 *6BB, United Kingdom*

6 **Corresponding author address: H.F.Dacre, Department of Meteorology, University of Reading,*
7 *Earley Gate, PO Box 243, Reading, RG6 6BB, United Kingdom.*

8 *E-mail: h.f.dacre@reading.ac.uk*

9 *†Current affiliation: Department of Meteorology, University of Reading, Earley Gate, PO Box 243,*
10 *Reading, RG6 6BB, United Kingdom.*

ABSTRACT

11 Volcanic ash poses an ongoing risk to the safety of airspace worldwide. The
12 accuracy to which we can forecast volcanic ash dispersion depends on the con-
13 ditions of the atmosphere into which it is emitted. In this paper we use mete-
14 orological ensemble forecasts to drive a volcanic ash transport and dispersion
15 model for the 2010 Eyjafjallajökull eruption. From analysis of these simu-
16 lations we determine why the skill of deterministic-meteorological forecasts
17 decrease with increasing ash residence time, and identify the atmospheric con-
18 ditions in which this drop in skill occurs most rapidly. Large forecast errors
19 are more likely when ash particles encounter regions of large horizontal flow
20 separation in the atmosphere. Nearby ash particle trajectories can rapidly di-
21 verge leading to a reduction in the forecast accuracy of deterministic forecasts
22 which do not represent variability in wind fields at the synoptic-scale. The
23 flow separation diagnostic identifies where and why large ensemble spread
24 may occur. This diagnostic can be used to alert forecasters to situations in
25 which the ensemble mean is not representative of the individual ensemble
26 member volcanic ash distributions. Knowledge of potential ensemble outliers
27 can be used to assess confidence in the forecast and to avoid potentially dan-
28 gerous situations in which forecasts fail to predict harmful levels of volcanic
29 ash.

30 **1. Introduction**

31 Volcanic ash poses a significant hazard to aircraft. It can cause both temporary engine failure
32 and permanent engine damage (*Guffanti et al. 2005*). Flights are therefore restricted in ash con-
33 taminated airspace, which disrupts air traffic leading to the potential for large financial losses. For
34 example the 2010 Eyjafjallajökull eruption grounded over 95,000 flights, costing the airline in-
35 dustry over 1 billion pounds. Analysis of the 1900-2010 Icelandic historical records shows that a
36 volcanic eruption of the size of the 2010 Eyjafjallajökull eruption has a repeat period of between
37 5 and 10 years (*Thordarson and Larson 2007*). Worldwide, volcanic eruptions 10 times the size
38 of the 2010 Eyjafjallajökull eruption have repeat periods on a decadal timescale (e.g. Mount St
39 Helens 1980, Hudson 1991, Puyehue 2011). Given the ongoing risk of volcanic eruptions it is
40 important to continually evaluate and improve the accuracy of volcanic ash forecasts to ensure
41 safe and optimised flight operations during future volcanic eruptions.

42 The volcanic ash advisory centres (VAACs) are responsible for producing volcanic ash cloud
43 analysis and forecasts to assist the aviation community in planning their operations and minimis-
44 ing risks. There are currently 9 VAACs that together provide a comprehensive global modelling
45 and warning system for the aviation community. These 9 VAACs use 6 different volcanic ash
46 transport and dispersion (VATD) models to to produce volcanic ash charts showing the forecast
47 location of volcanic ash in the atmosphere at different flight levels and out to forecast lead-times
48 of 24 hours. VATD models are initialised using data about the location of the eruption, the time
49 at which the eruption started and, if available, information about the plume rise height, vertical
50 profile of volcanic ash and ash size distribution (known collectively as eruption source parameters,
51 ESPs). They also use 3-D winds as input from numerical weather predictions to transport volcanic
52 ash away from the source. Typically the meteorological input used has a horizontal resolution of

53 between 10 and 50km. To represent dispersion on scales smaller than this horizontal diffusion
54 is applied. The diffusion represents the dispersion by unresolved eddies and acts to increase the
55 vertical and lateral spread of volcanic ash clouds (*Dacre et al. 2015*). This approach assumes
56 that the small-scale dispersion processes are of an eddy viscosity character and thus can be repre-
57 sented using a Gaussian description (*Pasquill and Smith 1983*). The simulated ash cloud therefore
58 represents the time mean of an ensemble of realisations.

59 At larger scales however, individual realisations can often display considerable deviations from
60 the ensemble mean (*Mylne and Mason 1991*). The scale at which this occurs depends on the
61 size of the dispersion processes relative to the width of the time averaged ash cloud. For aver-
62 aging periods of a few hours, this scale is typically greater than 500 km. Variability on synoptic
63 scales however differs for different atmospheric circulation patterns, meaning that the traditional
64 Gaussian diffusion approach used for small-scale dispersion processes cannot be used. Current
65 operational VATD models do not represent variability at the synoptic scale. They use meteorolog-
66 ical input from a single realisation of the flow field to produce a volcanic ash forecast (referred
67 to as *deterministic-met volcanic ash forecast* in this paper). The aim of this paper is to identify
68 the atmospheric conditions in which there is a higher chance that deterministic-met volcanic ash
69 forecast skill may rapidly decrease and to discuss the potential use of ensemble meteorological
70 input to VATD models as a method to address the missing synoptic-scale variability in volcanic
71 ash forecasts (referred to as *ensemble-met volcanic ash forecasts* in this paper).

72 Several studies have investigated the space and time-dependent skill of deterministic-met vol-
73 canic ash forecasts. For example, *Stunder et al. (2007)* analysed the forecast skill for 7 different
74 volcanic eruptions by comparing deterministic-met volcanic ash forecasts with satellite observa-
75 tions. They showed that these forecasts were generally good for short-term (18 hours from start
76 of the eruption) forecasts but that forecast skill appeared to decrease at longer lead-times. This

77 relationship between volcanic ash forecast skill and forecast lead-time is due to (i) increasing er-
78 rors in the forecast wind fields and ESPs at longer forecast lead-times and (ii) longer lead-time
79 forecasts include particles with longer residence times. These particles experience an accumula-
80 tion of errors in the wind field leading to larger positional errors on average than particles with
81 shorter residence times. *Dacre et al. (2016)* examined the second of these sources of error by per-
82 forming hindcast simulations of the Eyjafjallajökull eruption (using analysis wind fields). They
83 showed that generally skill decreases as the residence time of ash increases but that the rate of
84 skill decrease depends on the meteorological situation. In some situations only the position of ash
85 particles with residence time less than 24 hours are correctly simulated whereas in other situations
86 the position of ash particles with residence times longer than 72 hours can be accurately simulated.
87 Other studies have shown that the inclusion of buffer zones, to account for positional errors in the
88 deterministic-met volcanic ash clouds, can lead to significant improvement in the agreement with
89 observations (*Webster et al. 2012; Grant et al. 2012*). These buffer zones are a simplistic attempt
90 to account for uncertainty in the synoptic-scale wind fields.

91 For some time the use of ensemble-met volcanic ash forecasts has been advocated by the wider
92 volcanic ash community (*Bonadonna et al. 2012*) as a more rigorous way of accounting for uncer-
93 tainty in large-scale wind field. *Stefanescu et al. (2014)* and *Madankan et al. (2014)* include both
94 ensemble meteorology and an ensemble of ESPs in their study to quantify overall uncertainty in
95 volcanic ash forecasts. They demonstrate that the range of predicted concentrations can be large
96 at forecast lead-times of 48 hours. Similarly *Vogel et al. (2014)* performed time-lagged ensemble
97 simulations of volcanic ash dispersion from the Eyjafjallajökull plume and found that for some
98 times the spread in ensemble-met forecasts is small but at others it is large. They attribute this to
99 the nonlinear behaviour of the atmosphere. *Dare et al. (2016)* performed a comparison of both
100 deterministic and ensemble-met volcanic ash forecasts for the 2014 Kelut eruption. They found

101 that both showed good agreement with satellite observations for the first 12 hours from the start
102 of the eruption. However, for longer lead-times (18-24 hours) the ensemble-met forecast showed
103 better agreement with observations than the deterministic-met forecast.

104 While all these studies demonstrate that ensemble-met forecasts show better agreement with
105 observations than the deterministic-met forecasts, particularly at longer lead-times, the dynamical
106 reasons why they perform better has not been explored. The aim of our study therefore is to
107 illustrate why the skill of deterministic-met forecasts decreases with increasing ash residence time,
108 and furthermore to identify the atmospheric conditions in which this drop in skill occurs most
109 rapidly. These conditions are identified using ECMWF meteorological ensembles as input to the
110 NAME VATD model to simulate an ensemble of particle trajectories.

111 **2. Methodology**

112 *a. Meteorological fields*

113 In order to determine the uncertainty associated with the synoptic scale meteorological flow
114 field an ensemble of meteorological forecasts are used. Each forecast is produced from perturbed
115 initial conditions that represent the likely initial analysis error distribution. In this paper the Eu-
116 ropean Centre for Medium Range Weather Forecasting (ECMWF) Integrated Forecasting System
117 (cycle 41r1) has been used to create bespoke ensemble forecasts of the meteorological conditions
118 during the 2010 eruption of Eyjafjallajökull. Global forecasts are initialised every 12 hours be-
119 tween 00 UTC on 1 May - 12 UTC on 8 May 2010. Each forecast is 42 hours long and has
120 20 ensemble members. Data is archived every 6 hours on 26 levels and at T639 spectral trunca-
121 tion (approximately 32km horizontal grid spacing). Initial perturbations are constructed using the
122 singular-vector approach (*Buizza and Palmer 1995*) and model uncertainty is taken into account

123 through the use of a simple stochastic physics scheme (*Buizza et al.* 1995). Data is extracted from
124 the ECMWF archive at $0.25^\circ \times 0.25^\circ$ on a regular lat/lon grid and several fields (surface stresses,
125 sensible heat flux and precipitation fields) are post-processed as data extracted from the ECMWF
126 archive cannot be used directly as input to the VATD model described in section b.

127 *b. NAME dispersion simulations*

128 The VATD model used in this study is the Numerical Atmospheric-dispersion Modelling Envi-
129 ronment (NAME). NAME is used by the London Volcanic Ash Advisory centre to forecast the
130 spatial distribution of volcanic ash following an eruption. In this study we use NAME III (version
131 6.3) and ECMWF numerical weather prediction meteorological data to disperse particles released
132 into the atmosphere at the position of the Eyjafjallajökull volcano in Iceland. The dispersion of
133 volcanic ash by small-scale three-dimensional atmospheric turbulence and unresolved mesoscale
134 motions are parametrized within NAME using random-walk techniques. The aim of the random-
135 walk dispersion is to compute an ensemble of random trajectories of Lagrangian particles through
136 a flow field whose statistics are based on observations of vertical and horizontal velocity variances
137 and diffusivities (*Thomson and Wilson* 2013). The position of the particles is tracked for 42 hours
138 to create particle trajectories. The volcanic ash density is assumed to be 2300 kg m^{-3} based on the
139 value used in the operational version of NAME (*Leadbetter and Hort* 2011) and the particle size
140 is assumed to be $2 \mu\text{m}$ based on in-situ observations of the ash cloud by the FAAM aircraft over
141 and around the UK in the Eyjafjallajökull ash cloud (*Johnson et al.* 2012). Particles are subject to
142 removal processes including sedimentation, wet and dry deposition (*Jones et al.* 2007). Note that
143 the choice of particle size does not affect the conclusions reached in the paper.

144 *c. SEVIRI satellite observations*

145 To qualitatively evaluate the performance of the NAME forecasts we compare simulated ash
146 cloud distributions with data from the Spinning Enhanced Visible and Infrared imager (SEVIRI).
147 SEVIRI volcanic ash retrievals are calculated using brightness temperature difference measure-
148 ments (see *Francis et al. (2012)* for more details). The advantage of using volcanic ash retrievals
149 from an instrument onboard a geostationary satellite is that they are available at high temporal res-
150 olution, every hour, allowing us to track the evolution of the volcanic ash cloud and to interpolate
151 between timesteps when water or ice clouds obscure the volcanic ash. Following the method of
152 *Harvey and Dacre (2016)* we composite satellite observations over a 5 hour time window. This has
153 been shown to be sufficient to create a continuous time series while remaining highly correlated
154 with the noncomposited fields. The satellite volcanic ash retrievals are averaged onto a $0.5^\circ \times 0.5^\circ$
155 latitude/longitude grid to allow direct comparison with the NAME output.

156 *d. Ensemble spread and flow separation diagnostics*

157 One measure of the uncertainty in meteorological flow conditions is the time evolution of spatial
158 spread in particle trajectories. In this paper the ensemble spread is calculated using the root-
159 mean-square (*RMS*) distance between individual ensemble particle positions (1 particle from each
160 ensemble simulation), (\mathbf{x}_i) , and the mean position of the particles, $(\bar{\mathbf{x}}_i)$, summed over all N particles
161 (thus N equals 20 as there are 20 ensemble simulations). The distance is measured perpendicular
162 to the mean direction travelled by the particles during the previous 10 minutes to capture lateral
163 spreading of the trajectories only.

$$RMS = \sqrt{\frac{1}{N} \sum_i^N (\mathbf{x}_i - \bar{\mathbf{x}}_i)^2} \quad (1)$$

164 The diagnostic used to characterise the synoptic-scale flow conditions is the 2-D horizontal flow
 165 separation diagnostic introduced in *Dacre et al.* (2016). This flow separation is calculated as the
 166 velocity gradient perpendicular to the flow.

$$\frac{\partial \mathbf{v}}{\partial n} = \frac{1}{q^2} \left[v^2 \frac{\partial u}{\partial x} - uv \left(\frac{\partial u}{\partial y} + \frac{\partial v}{\partial x} \right) + u^2 \frac{\partial v}{\partial y} \right] \quad (2)$$

167 where \mathbf{v} is the velocity vector, q is the wind speed, n is distance in the direction perpendicular to
 168 the flow, and x and y are distances in longitude and latitude directions, respectively. Where this
 169 diagnostic is positive, the atmospheric flow separates, and where it is negative, the flow contracts.
 170 Thus it is a good diagnostic for identifying where particle trajectories will spread apart. The flow
 171 separation diagnostic is related to the 3-D Lyapunov exponents used by *Legras et al.* (2005) and
 172 *Pisso and Legras* (2008) to characterise the rate of separation of infinitesimally close trajectories
 173 in phase space.

174 3. Results

175 a. Satellite-detected ash clouds

176 Figure 1(a) and (b) show the ash cloud from the Eyjafjallajökull eruption, as detected by the
 177 SEVIRI instrument. At 12 UTC on 7 May (figure 1(a)) the ash was detected in a coherent plume
 178 extending southward from Iceland to the west of the UK. The ash cloud exhibits an anticyclonic
 179 curvature as ash particles were transported anticyclonically around a high-pressure centre in the
 180 North-Atlantic. At around 50°N the ash cloud has started to bifurcate with one branch of volcanic
 181 ash continuing to follow an anticyclonic trajectory whilst another branch was advected cycloni-
 182 cally towards southern Europe. This cyclonic branch reaches the coast of Portugal at 00 UTC
 183 on the 8 May (figure 1(b)) whilst the majority of the volcanic ash continues to travel anticycloni-
 184 cally. The ability of VATD models to capture this complex ash cloud bifurcation is dependent on

185 the accurate representation of the input meteorological wind fields. For example, *Wilkins et al.*
186 (2016) showed that their NAME deterministic-met volcanic ash forecast was not able to capture
187 the structure the thin filament of ash extending over northern Spain on 8 May 2010.

188 *b. Ensemble member forecasts*

189 Figures 1(c),(d) and (e),(f) show two volcanic ash forecasts using different ECMWF ensemble
190 member flow fields, both initialised at 00 UTC on 6 May 2010. Particles are released at the loca-
191 tion of Eyjafjallajökull volcano at a rate of 3600/hr. All of the particles were released at a height
192 consistent with the maximum observed plume height at that time. It can be seen that close to the
193 volcano the volcanic ash distribution for both forecasts is very similar, with both forecasts pro-
194 ducing an ash cloud extending southward from Iceland to the west of the UK, consistent with the
195 satellite detected ash cloud location. However, at 50°N the forecasts start to diverge. In figures 1(e)
196 and (f) the majority of the volcanic ash is transported cyclonically and is advected towards Europe.
197 In contrast in figures 1(c) and (d) the majority of the volcanic ash cloud continues to travel anticy-
198 clonically and is advected into the North Atlantic. For this example, the deterministic-met forecast
199 shown in figures 1(c) and (d) would be considered a good forecast as it closely matches the evo-
200 lution of the ash cloud seen in the satellite observations. However the deterministic-met forecast
201 shown in figures 1(e) and (f) would be considered a poor forecast as it does not forecast the ob-
202 served ash in the North Atlantic. This is despite both forecasts using equally plausible realisations
203 of the flow field. This example highlights the danger of using a single deterministic-met flow field
204 as input to a VATD model to forecast the ash cloud distribution. These 2 ensemble members are
205 chosen because they exhibit very different volcanic ash cloud evolutions, the other 18 ensemble
206 members result in ash distributions which resemble a mixture of the two extremes.

207 *c. Flow separation*

208 In this section we explain why the ensemble member forecasts differ so much from each other.
209 In order to do this we examine the flow pattern at approximately 50°N and 15°W, the location at
210 which the ash particle trajectories show an increase in spread.

211 Figures 2(a) and (b) shows the streamlines and flow separation at 12UTC and 18UTC on 6 May
212 respectively, for a single deterministic-met ensemble member forecast. The streamlines evolve
213 over time but broadly show a low pressure to the west of the domain, a large region of high
214 pressure in the centre of the domain and low pressure in the east of the domain. Figures 2(a) and
215 (b) also show the flow separation diagnostic averaged over 100hPa at the release height of the ash
216 particles. The flow separation is positive in regions where the streamlines spread apart and negative
217 where the streamlines contract. For the purposes of illustrating why different ensemble members
218 diverge and under what conditions, it is not feasible to visualise the trajectories of thousands of
219 particles. Therefore, for simplicity, we have chosen to visualise a single particle trajectory (that is
220 not subject to stochastic motions) from each ensemble member. The thick black trajectory shown
221 in figures 2(a) and (b) is a single 42 hr particle trajectory from the same ensemble simulation shown
222 in figure 1(e) and (f)). This particle was released from the volcano source at 06 UTC and is subject
223 to the flow field shown in figures 2(a) and (b). In order to isolate transport by the resolved-scale
224 flow it is not subject to perturbations representing unresolved eddies, hence its smooth trajectory.
225 The black star indicates the location of the particle at the time of the flow separation field. 12 hours
226 after the particle is released into the atmosphere (figure 2(a)) the particle is at 57°N, 13°W where
227 the streamlines are roughly parallel to one another and hence flow separation is small. 24 hours
228 after the particle is released into the atmosphere (figure 2(b)) the particle is at 51°N, 17°W and is

229 in a region of strong positive flow separation. The streamlines spread apart as they approach the
230 point of intersection between the trough and ridge region (known as a col or saddle point).

231 It is difficult to analyse the along-trajectory flow separation in this Eulerian framework, therefore
232 figure 2(c) shows the flow separation extracted at the relevant time along the Lagrangian particle
233 trajectory. This Lagrangian analysis demonstrates that the particle advected in this deterministic-
234 met forecast enters a region of strong flow separation at 52°N , 17°W . In order to determine whether
235 this is specific to a single ensemble-met member forecast or to all of the meteorological ensemble
236 forecasts initialised at 06UTC on 6 May the along-trajectory flow separation has been calculated
237 for each of the meteorological ensemble forecast members. Figure 2(d) shows the evolution of
238 flow separation along 20 particle trajectories released at the same time, a single particle trajectory
239 in each ensemble-met forecast. The flow separation in each ensemble-met forecast is very similar
240 up until the point at which the trajectories start to diverge. This is expected since the regions of
241 positive and negative flow separation are spatially coherent. It also illustrates how the trajectory
242 separation rapidly increases after the point at which the trajectories encounter the region of positive
243 flow separation. Performing an ensemble-met volcanic ash forecast for this case accounts for the
244 variability in the synoptic flow field and is necessary to fully encompass the ash cloud distribution
245 uncertainty due to the flow field.

246 *d. Trajectory spread*

247 To establish if trajectory spreading always rapidly increases after trajectories encounter regions
248 of positive flow separation similar experiments were performed for meteorological ensemble fore-
249 casts initialised at 06UTC on the 15 April - 7 May 2010. For each of these ensemble forecasts a
250 single particle were released at a height corresponding to the observed plume top from the Eyjaf-
251 jallajökull volcano. It is well known that in low wind-speed conditions wind direction can vary

252 significantly in a short period of time causing particle trajectories can rapidly diverge (*Venkatram*
253 *et al.* 2004). In this paper we choose to focus on the less well studied uncertainty occurring in
254 moderate-strong wind conditions and thus only analyse the situations in which the wind speed at
255 the release height was greater than 10m s^{-1} . Figure 3 shows the ensemble-met member forecasts
256 with the 4 highest (figures 3(a)-(d)) and 4 lowest (figures 3(e)-(h)) trajectory spreads. Individual
257 particle trajectories correspond to a single particle released at the same time in each ensemble-met
258 member forecast. It can be seen that on some days, figures 3(a)-(d), the trajectories diverge after
259 encountering regions of positive flow separation, consistent with the analysis for the 6 May 2010
260 (figures 2(d)). By comparison on other days, figures 3(e)-(h) the trajectories remain close together
261 for 42 hours.

262 Figure 4 quantitatively describes the relationship between residence time and ensemble-met
263 forecast trajectory spread (measured using the RMS perpendicular distance described in section d).
264 As observed in figure 3 trajectory spread generally increases with residence time but not always at
265 the same rate. The rate of trajectory spread depends on the synoptic situation. Figure 4 also shows
266 the maximum along-trajectory flow separation from each ensemble-met forecast, accumulated
267 over 42 hours for each set of simulations. The simulation with the smallest trajectory spread after
268 42 hours residence time corresponds to the 3 May 2010 (figure 3(h)) and the along-trajectory
269 accumulated flow separation is small at all points along the trajectory. By contrast the simulation
270 with the largest trajectory spread corresponds to the 19 April 2010 (figure 3(a)) and the along-
271 trajectory accumulated flow separation is neutral or positive at all points along the trajectory. Thus,
272 these simulations suggest that trajectories that experience large along-trajectory accumulated flow
273 separation are more likely to spread apart than trajectories that experience no large along-trajectory
274 flow separation, potentially leading to large error growth for a single deterministic forecast (as
275 shown in figure 1)

276 **4. Discussion and Conclusions**

277 In this paper we examine the atmospheric flow characteristics that lead to volcanic ash cloud
278 bifurcation and a reduction in forecast skill. We performed multiple forecasts using the UK Met
279 Office volcanic ash transport and dispersion model (NAME) and input from ensemble meteorological
280 flow fields from the ECMWF ensemble prediction system.

281 In moderate to strong wind situations the atmospheric conditions leading to large variability
282 in volcanic ash particle positions are associated with large flow separation. When ash particles
283 encounter regions of large horizontal flow separation their future trajectories are very sensitive
284 to their position at that time. Nearby ash particle trajectories can rapidly diverge leading to a
285 reduction in forecast accuracy for deterministic-met volcanic ash forecasts. Potentially leading to
286 predictions of ash-free airspace in regions that are in-reality contaminated with ash or vice versa.

287 In order to fully represent the synoptic-scale meteorological uncertainty ensemble-met volcanic
288 ash forecasts are needed. When volcanic ash clouds encounter regions of large flow separation the
289 individual ensemble-met members may display considerable deviations from the ensemble mean.
290 2-D fields of positive flow separation could be used as a flag to alert forecasters to this potential
291 risk and the individual ensemble-met member forecasts analysed. A combination of the flow
292 separation diagnostic and ensemble volcanic ash forecasts will help to identify where and why
293 large uncertainty in the forecast occurs and provide an estimate of the confidence of the forecast.
294 For example, a forecaster could reduce the size of the hazardous area whenever high confidence
295 in the ash cloud forecast was indicated. Reductions in the hazard area would avoid unnecessary
296 disruption to airspace.

297 In this paper we have only considered the uncertainty in the horizontal wind fields. Uncertainty
298 also exists in the magnitude and location of precipitation which leads to wet-deposition of volcanic

299 ash. This uncertainty may also cause large errors in the magnitude of volcanic ash forecasts as
300 precipitation is a very efficient removal mechanism. We have also not considered the uncertainty
301 associated with the volcanic eruption source parameters (ESPs). The best way to combine the
302 meteorological and ESP uncertainty and effective ways of communicating this uncertainty with
303 users is the subject of future work.

304 *Acknowledgments.* We are grateful to Pete Francis and Mike Cooke at the UK Met Office for
305 making their satellite derived volcanic ash data available. We also acknowledge use of ECMWF's
306 computing and archive facilities. Natalie Harvey gratefully acknowledges funding from NERC
307 grant NE/J017221/1 Probability, Uncertainty and Risk in the Environment. We thank Andrew
308 Jones at the UK Met Office for his help in performing the NAME ensemble simulations and
309 Alan Grant and Peter Clark for useful discussions on this work. The SEVIRI satellite data
310 and NAME simulation output are available in University of Reading Research Data Archive,
311 <http://dx.doi.org/10.5072/uor-data-00000000>. Further information about the data supporting these
312 findings and requests for access to the data can be directed to h.f.dacre@reading.ac.uk.

313 **References**

314 **References**

315 Bonadonna, C., Folch, A., Loughlin, S. and Puempel, H., (2012). Future developments in mod-
316 elling and monitoring of volcanic ash clouds: outcomes from the first IAVCEI-WMO workshop
317 on Ash Dispersal Forecast and Civil Aviation. *Bulletin of volcanology* 74, 1-10.

318 Buizza, R. and Palmer, T.N., (1995). The singular-vector structure of the atmospheric global cir-
319 culation. *Journal of the Atmospheric Sciences* 52, 1434-1456.

320 Buizza, R., Milleer, M. and Palmer, T.N., (1999). Stochastic representation of model uncertainties
321 in the ECMWF ensemble prediction system. *Quarterly Journal of the Royal Meteorological*
322 *Society* 125, 2887-2908.

323 Dacre, H.F., Harvey, N.J., Webley, P.W. and Morton, D., (2016). How accurate are volcanic ash
324 simulations of the 2010 Eyjafjallajökull eruption? *Journal of Geophysical Research: Atmo-*
325 *spheres* 121, 3534-3547.

326 Dacre, H.F., Grant, A.L.M., Harvey, N.J., Thomson, D.J., Webster, H.N. and Marenco, F., (2015).
327 Volcanic ash layer depth: Processes and mechanisms. *Geophysical Research Letters* 42, 637-
328 645.

329 Dare, R.A., Smith, D.H. and Naughton, M.J., (2016). Ensemble Prediction of the Dispersion of
330 Volcanic Ash from the 13 February 2014 Eruption of Kelut, Indonesia. *Journal of Applied Me-*
331 *teorology and Climatology* 55, 61-78.

332 Francis, P. N., M. C. Cooke, and R. W. Saunders (2012). Retrieval of physical properties of vol-
333 canic ash using Meteosat: A case study from the 2010 Eyjafjallajökull eruption. *Journal of*
334 *Geophysical Research*, 117, D20, doi:10.1029/2011JD016788.

335 Grant, A.L., Dacre, H.F., Thomson, D.J. and Marenco, F., (2012). Horizontal and vertical structure
336 of the Eyjafjallajökull ash cloud over the UK: a comparison of airborne lidar observations and
337 simulations. *Atmospheric Chemistry and Physics* 12, 10145-10159.

338 Guffanti, M., Ewert, J.W., Gallina, G.M., Bluth, G.J. and Swanson, G.L., (2005). Volcanic-ash
339 hazard to aviation during the 2003-2004 eruptive activity of Anatahan volcano, Commonwealth
340 of the Northern Mariana Islands. *Journal of Volcanology and Geothermal Research* 146, 241-
341 255.

342 Harvey, N. J. and Dacre, H. F. (2016). Spatial evaluation of volcanic ash forecasts using satellite
343 observations (2016)*Atmos. Chem. Phys.* 16, 861-872.

344 Johnson, B., Turnbull, K., Brown, P., Burgess, R., Dorsey, J., Baran, A.J., Webster, H., Haywood,
345 J., Cotton, R., Ulanowski, Z. and Hesse, E., (2012). In situ observations of volcanic ash clouds
346 from the FAAM aircraft during the eruption of Eyjafjallajkull in 2010. *Journal of Geophysical*
347 *Research: Atmospheres*, 117, D20.

348 Jones, A., Thomson, D., Hort, M. and Devenish, B., (2007). The UK Met Office's next-generation
349 atmospheric dispersion model, NAME III *Air Pollution Modeling and its Application XVII*, 580-
350 589. Springer US.

351 Leadbetter, S.J. and Hort, M.C., (2011). Volcanic ash hazard climatology for an eruption of Hekla
352 Volcano, Iceland. *Journal of Volcanology and Geothermal Research*, 199, 230-241.

353 Legras, B., Pisso, I., Lefevre, F., and Berthet, G. (2005). Lagrangian turbulent diffusion in the
354 lower stratosphere *Atmos.Chem. Phys.*, 5, 1605-1622.

355 Madankan, R., Pouget, S., Singla, P., Bursik, M., Dehn, J., Jones, M., Patra, A., Pavolonis, M.,
356 Pitman, E.B., Singh, T. and Webley, P., (2014). Computation of probabilistic hazard maps and
357 source parameter estimation for volcanic ash transport and dispersion. *Journal of Computational*
358 *Physics* 271, 39-59.

359 Mylne, K.R. and Mason, P.J., (1991). Concentration fluctuation measurements in a dispersing
360 plume at a range of up to 1000 m. *Quarterly Journal of the Royal Meteorological Society*, 117,
361 177-206.

362 Pasquill F. and Smith, F. B. (1983). *Atmospheric Diffusion*, third edition, Ellis Horwood, Chich-
363 ester.

- 364 Pisso, I. and Legras, B. (2008). Turbulent vertical diffusivity in the sub-tropical stratosphere *At-*
365 *mos. Chem. Phys.*, 8, 697-707.
- 366 Stefanescu, E. R., Patra, A. K, Bursik, M. I., Madankan, R., Pouget, S., Jones, M., Singla, P.,
367 Singh, T., Pitman, E. B., Pavolonis, M., Morton, D., Webley, P. and Dehn, J. (2014). Temporal,
368 probabilistic mapping of ash clouds using wind field stochastic variability and uncertain erup-
369 tion source parameters: Example of the 14 April 2010 Eyjafjallajökull eruption. *J. Adv. Model.*
370 *Earth Syst* 6, 1173-1184, doi:10.1002/2014MS000332.
- 371 Stunder, B.J., Heffter, J.L. and Draxler, R.R. (2007), Airborne volcanic ash forecast area reliability.
372 *Weather and Forecasting* 22, 1132-1139.
- 373 Thomson, D.J. and Wilson, J.D., (2013). History of Lagrangian stochastic models for turbulent dis-
374 persion. *Lagrangian modelling of the atmosphere, Geophysical Monograph Series 200, Ameri-*
375 *can Geophysical Union*, 19-36.
- 376 Thordarson, T. and Larsen, G. (2007), Volcanism in Iceland in historical time: Volcano types,
377 eruption styles and eruptive history. *Journal of Geodynamics* 43, 118-152.
- 378 Webster, H. N., Thomson, D. J., Johnson, B. T., Heard, I. P. C., Turnbull, K., Marengo, F.,
379 Kristiansen, N. I., Dorsey, J., Minikin, A., Weinzierl, B., Schumann, U., Sparks, R. S. J.,
380 Loughlin, S. C., Hort, M. C., Leadbetter, S. J., Devenish, B. J., Manning, A. J., Witham,
381 C. S., Haywood, J. M., and Golding, B. W. (2012), Operational prediction of ash concentra-
382 tions in the distal volcanic cloud from the 2010 Eyjafjallajökull eruption, *J. Geophys. Res.* 117,
383 DOI:10.1029/2011JD016790.
- 384 Venkatram, A., Isakov, V., Yuan, J., and Pankratz, D. (2004). Modeling dispersion at distances of
385 meters from urban sources. *Atmospheric Environment* 38, 4633-4641.

386 Vogel, H., Förstner, J., Vogel, B., Hanisch, T., Mühr, B., Schättler, U. and Schad, T. (2014). Time-
387 lagged ensemble simulations of the dispersion of the Eyjafjallajökull plume over Europe with
388 COSMO-ART. *Atmospheric Chemistry and Physics* 14, 7837-7845.

389 Wilkins, K. L., I. M. Watson, N. I. Kristiansen, H. N. Webster, D. J. Thomson, H. F. Dacre and A.
390 J. Prata (2016). Using data insertion with the NAME model to simulate the 8 May 2010 Eyjafjal-
391 lajökull volcanic ash cloud, *Journal of Geophysical Research*, 121, doi:10.1002/2015JD023895.

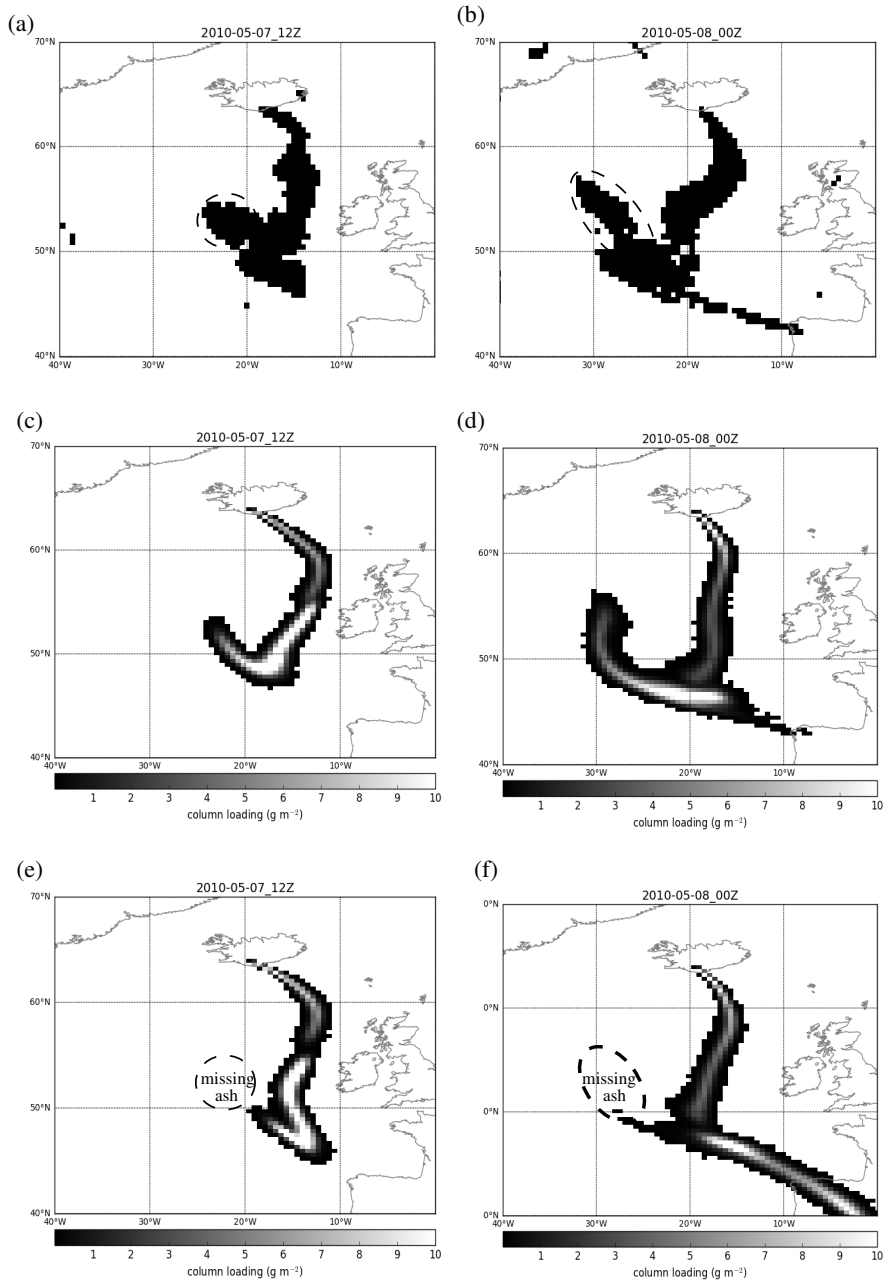
392 **LIST OF FIGURES**

393 **Fig. 1.** 5 hour composite of satellite-detected ash clouds at (a) 12 UTC on 7 May, (b) 00 UTC on
394 8 May 2010. (c)-(f) show ash column loading forecasts for two ensemble member forecasts
395 both initialised at 06 UTC on 6 May 2010. (c),(e) valid at 12 UTC on 7 May, (d),(f) valid at
396 00 UTC on 8 May 2010 21

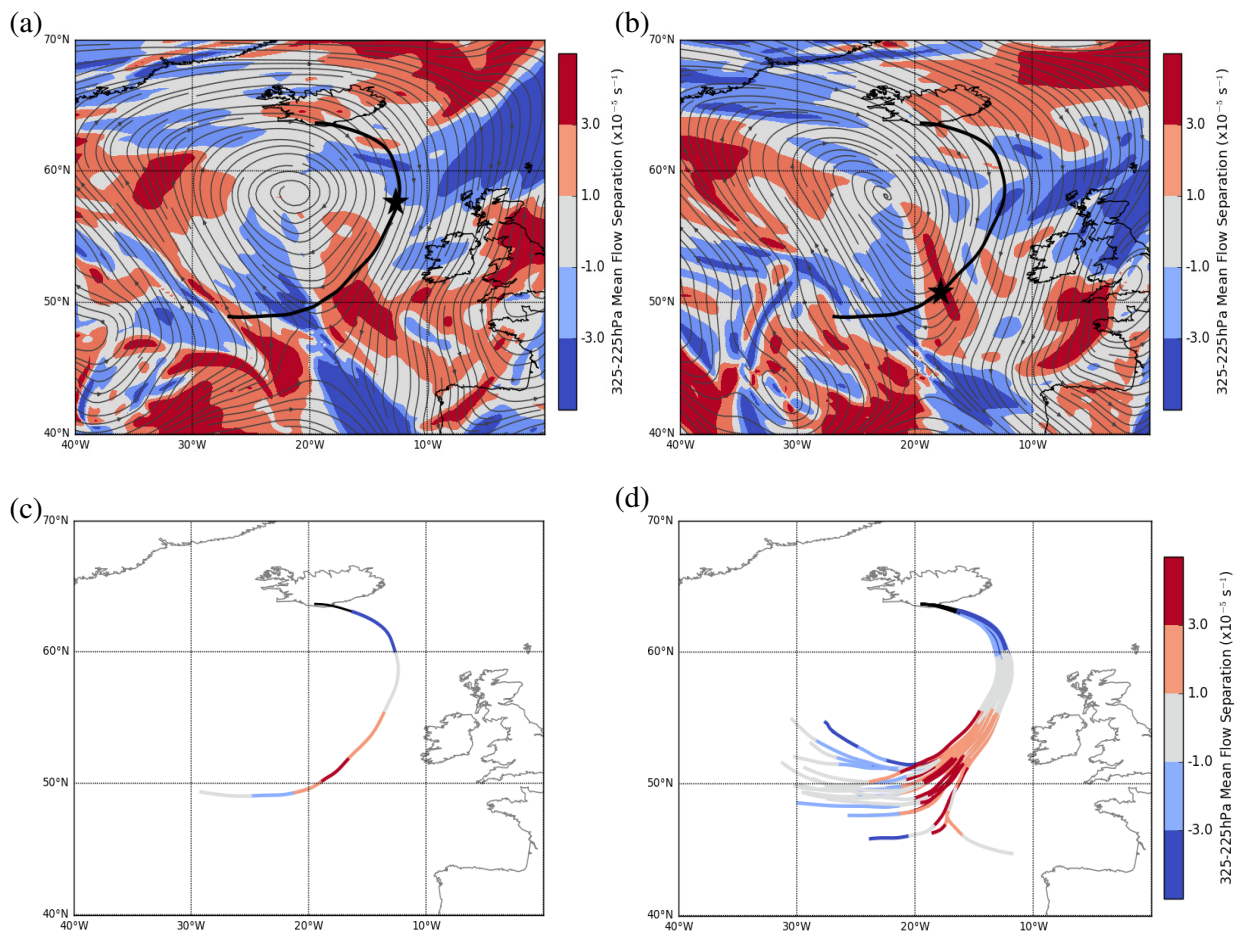
397 **Fig. 2.** Flow separation averaged from 325-225hPa (filled contours) overlaid with 275hPa stream-
398 lines (grey) at (a) 18TUC on 6 May 2010, and (b) 06 UTC on 7 May 2010. 42hr particle
399 trajectory initialised at 06 UTC on 6 May 2010 (thick black line) and position of particle at
400 time of flow separation and streamline fields (black star). (c) Flow separation along the par-
401 ticle trajectory shown in (a) and (b) from 12 hrs residence time onwards. (d) Flow separation
402 along 20 particle trajectories advected by 20 different forecast wind fields. 22

403 **Fig. 3.** Ash particle trajectories for 42 hour forecasts with perturbed initial conditions. Forecasts
404 with the highest trajectory spread after 42 hours (a)-(d) and lowest trajectory spread after 42
405 hours (e)-(h). Colours show 6-hourly averaged flow separation. 23

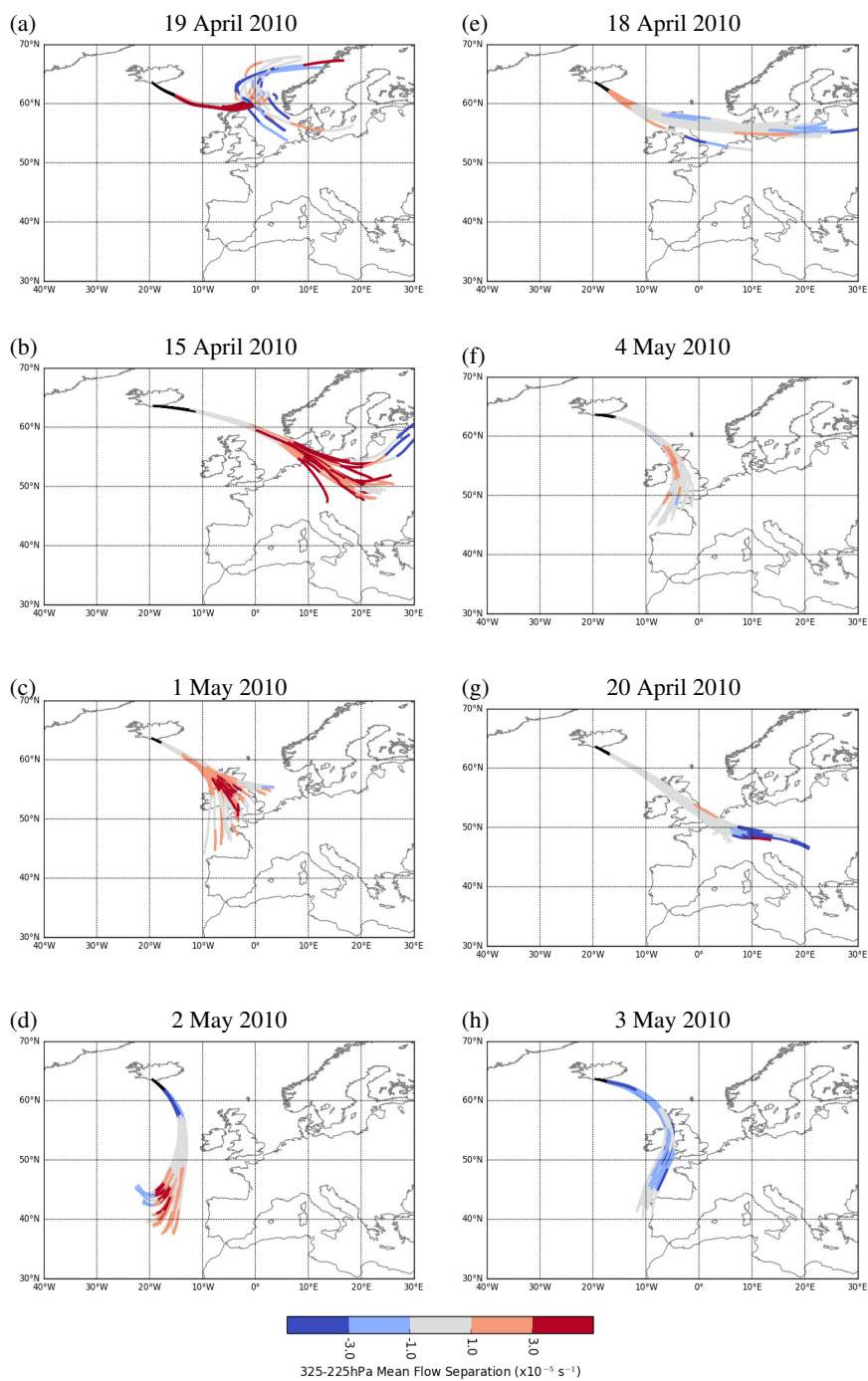
406 **Fig. 4.** Evolution of ensemble spread for 14 simulations initialised at 06UTC between 15 April and
407 7 May 2010. Colours show the along-trajectory accumulated maximum flow separation. 24



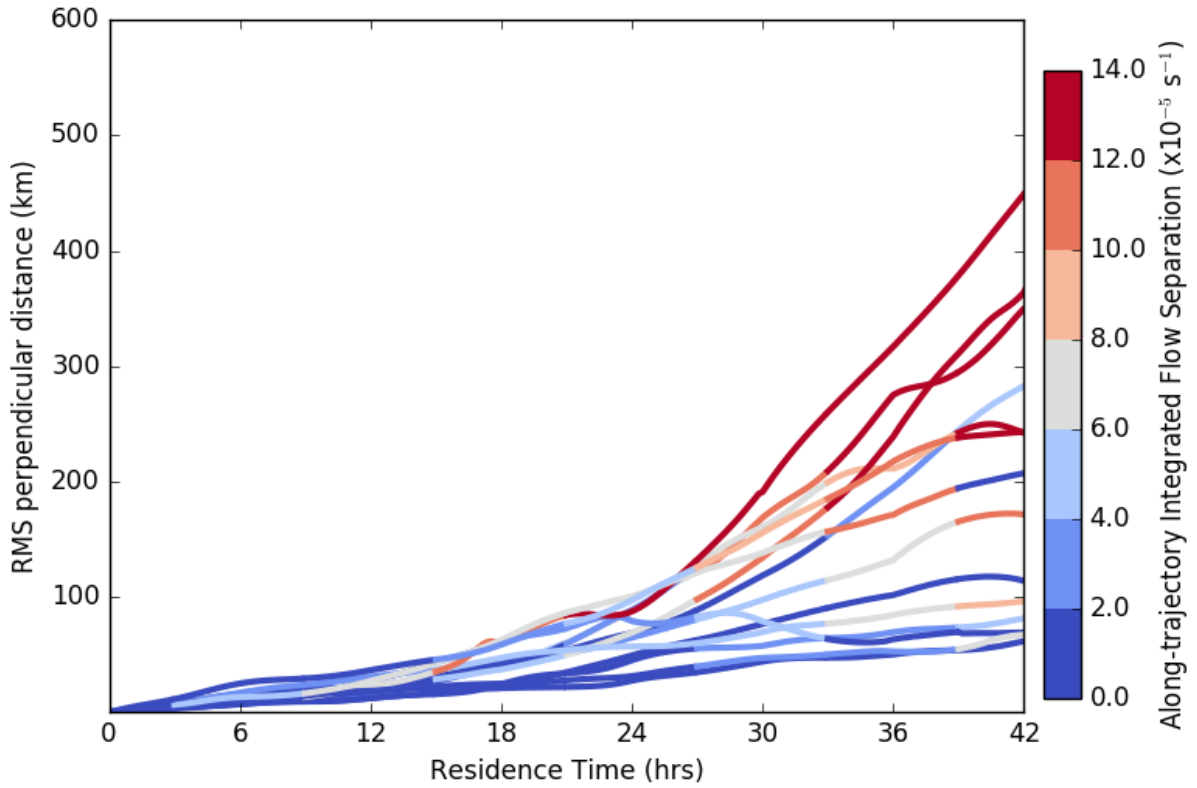
408 FIG. 1. 5 hour composite of satellite-detected ash clouds at (a) 12 UTC on 7 May, (b) 00 UTC on 8 May 2010.
 409 (c)-(f) show ash column loading forecasts for two ensemble member forecasts both initialised at 06 UTC on 6
 410 May 2010. (c),(e) valid at 12 UTC on 7 May, (d),(f) valid at 00 UTC on 8 May 2010



411 FIG. 2. Flow separation averaged from 325-225hPa (filled contours) overlaid with 275hPa streamlines (grey)
 412 at (a) 18TUC on 6 May 2010, and (b) 06 UTC on 7 May 2010. 42hr particle trajectory initialised at 06 UTC
 413 on 6 May 2010 (thick black line) and position of particle at time of flow separation and streamline fields (black
 414 star). (c) Flow separation along the particle trajectory shown in (a) and (b) from 12 hrs residence time onwards.
 415 (d) Flow separation along 20 particle trajectories advected by 20 different forecast wind fields.



416 FIG. 3. Ash particle trajectories for 42 hour forecasts with perturbed initial conditions. Forecasts with the
 417 highest trajectory spread after 42 hours (a)-(d) and lowest trajectory spread after 42 hours (e)-(h). Colours show
 418 6-hourly averaged flow separation.



419 FIG. 4. Evolution of ensemble spread for 14 simulations initialised at 06UTC between 15 April and 7 May
 420 2010. Colours show the along-trajectory accumulated maximum flow separation.